The Role of Seven Coordination in Ru-catalyzed Water Oxidation

Roc Matheu,[a,b] Mehmed Z. Ertem,[c] Muriel Pipelier,[e] Jacques Lebreton,[e] Didier Dubreuil,[e] Jordi Benet-Buchholz,[a] Xavier Sala,[d] Arnaud Tessier*[,e] and Antoni Llobet* [a,d]

[a] Institute of Chemical Research of Catalonia (ICIQ), Barcelona Institute of Technology (BIST), Avinguda Països Catalans 16, 43007 Tarragona, Spain.

[b] Departament de Química Física i Inorgànica, Universitat Rovira i Virgili, Marcel·lí Domingo s/n, 43007 Tarragona, Spain.

[c] Chemistry Division, Energy & Photon Sciences Directorate, Brookhaven National Laboratory, Upton, New York, 11973-5000, USA

[d] Departament de Química, Universitat Autònoma de Barcelona, Cerdanyola del Vallès, 08193 Barcelona, Spain.

[e] Université de Nantes, CNRS, CEISAM, UMR 6230, Faculté des Sciences et des Techniques, 2 rue de la Houssinière, BP 92208, 44322 Nantes, France.

Corresponding authors: Arnaud.Tessier@univ-nantes.fr; allobet@iciq.es

Abstract

A family of Ru complexes based on the pentadentate t5a^{3-} ligand ((2,5-bis(6-carboxylatopyridin-2-yl)pyrrol-1-ide) and pyridine (py) that include, {Ru^{II}(Ht5a-κ-N^{2}O)(py)$_3$}, **1**H^{II}(κ-N^{2}O), {Ru^{III}(t5a-κ-N^{3}O$^{1.5}$)(py)$_2$}, **2**^{III}(κ-N^{3}O$^{1.5}$) and {Ru^{IV}(t5a-κ-N^{3}O^2)(py)$_2$}$^+$, {**2**^{IV}(κ-N^{3}O^2)}$^+$ has been prepared and thoroughly characterized. Complexes **1**H^{II}(κ-N^{2}O), **2**^{III}(κ-N^{3}O$^{1.5}$) and {**2**^{IV}(κ-N^{3}O^2)}$^+$ have been investigated in solution by spectroscopic methods (NMR, UV-vis) and in the solid state by single-crystal X-ray diffraction analysis and complemented by density functional theory (DFT) calculations. The redox properties of complex **2**^{III}(κ-N^{3}O$^{1.5}$) have been studied by electrochemical methods (CV and DPV), showing its easy access to high oxidation states, thanks to the trianionic nature of the t5a^{3-} ligand. In neutral to basic conditions complex {**2**^{IV}(κ-N^{3}O^2)}$^+$ undergoes aquation generating {Ru^{IV}(OH)(t5a-κ-N^{2}O)(py)$_2$}, **2**^{IV}(OH)(κ-N^{2}O). Further oxidation of the complex forms {Ru^{V}(O)(t5a-κ-N^{2}O)(py)$_2$}, **2**^{V}(O)(κ-N^{2}O) that is a very efficient water oxidation catalyst, reaching TOF$_{MAX}$ of 9400 s^{-1} at pH = 7.0, as measured via foot of the wave analysis. The key to fast kinetics for the catalytic oxidation of water to dioxygen by **2**^{V}(O)(κ-N^{2}O) is due to not only the easy access to high oxidation states but also to the intramolecular hydrogen bonding provided by the non-coordinated dangling carboxylate at the transition state, as corroborated by DFT calculations.

Keywords

Ru complexes, seven coordination, adaptative ligands, redox properties, water oxidation catalysis, electrocatalysis

1. Introduction

The future energetic scenario relies on our capacity to generate technologies that can store solar energy into chemical bonds.[1,2,3] This so called artificial photosynthesis requires catalysts that efficiently reduce abundant substrates such as H_2O, CO_2 or N_2 to hydrogen, hydrocarbons or NH_3 respectively that obtained in this way are named solar fuels.[4,5,6,7] An ideal partner for these reductions is the challenging $4e^-/4H^+$ oxidation of H_2O to O_2 that again requires efficient catalysts.[8,9,10] Recent advances on molecular water oxidation catalysis (WOC) based on Ru complexes, has generated an impressively detailed understanding of their mode of action and as a result robust WOCs with spectacular efficiencies have been achieved.[11,12,13] This understanding has been accomplished thanks to electrochemical, kinetic and spectroscopic characterization of reaction intermediates complemented with density functional theory (DFT) calculations.[11,12,14,15,16,17]

Ru complexes containing the equatorial bda^{2-} ([2,2'-bipyridine]-6,6'-dicarboxylate) and tda^{2-} ([2,2':6',2''-terpyridine]-6,6''-dicarboxylate) ligands are the fastest molecular water oxidation catalysts described so far in the literature (see Chart 1 for the ligand drawings).[12,18,19,20] The most paradigmatic Ru-bda complex is $\{Ru^{V}(O)(bda)(Me\text{-}py)_2\}^+$, $\{\mathbf{5}^{V}(O)\}^+$, where two 4-picoline (Me-py) ligands coordinate as axial ligands. Similarly, complex $\{Ru^{V}(O)(tda\text{-}\kappa\text{-}N^3O)(py)_2\}^+$, $\{\mathbf{3}^{V}(O)\}^+$, that bears two pyridines (py) in the axial positions is the most representative Ru-tda complex, see Table 1 for a drawing of these complexes. The two families of complexes can oxidize water at maximum turn over frequencies (TOF_{MAX}) between 10^3 s^{-1} and 10^4 s^{-1}, which exceed by 1-2 orders of magnitude the oxygen evolving catalyst in the natural photosystem II.[17,20,21] Two crucial features render Ru-bda and Ru-tda type of complexes as the best performing water oxidation catalysts in the literature. In the first place, the capacity of the carboxylato moieties in bda^{2-} and tda^{2-} ligands to form intramolecular hydrogen bonds with the active Ru-OH group at different oxidation states, which is beneficial for catalysis in terms of both thermodynamics and kinetics.[12,22,23] Secondly, the other key feature of tda^{2-} and bda^{2-} ligands is their capacity to stabilize Ru high oxidation states via the anionic character of the carboxylato groups (see Table 1 for the Ru-bda and Ru-tda structures) and also via the formation of seven coordination (CN7) beyond oxidation state IV. This stabilization reduces the overpotential (η) for the catalytic reaction up to 740 mV compared to other mononuclear Ru complexes bearing neutral polypyridine type of ligands with classical octahedral coordination.[12,23] The main challenge in the field of molecular water oxidation catalysis is to generate fast and oxidatively robust catalysts that operate at low overpotentials. Given the beneficial stabilization of the seven-coordination in lowering overpotentials, a question that unavoidably arises is whether CN7 indispensable for fast catalysis.[12,19,23,24]

Here on we present the synthesis, spectroscopic, electrochemical and catalytic properties of $\{Ru^{V}(O)(t5a\text{-}\kappa\text{-}N^2O)(py)_2\}$, $\mathbf{2}^{V}(O)(\kappa\text{-}N^2O)$, where $t5a^{3-}$ is 2,5-bis(6-carboxylatopyridin-2-yl)pyrrol-1-ide (see Chart 1). The $t5a^{3-}$ ligand is a pentadentate ligand that can occupy the equatorial positions of a transition metal center with a pentagonal bipyramid type of geometry. Further, it contains three anionic charges, one from the pyrrolato group and two from the carboxylatos, where the latter can also provide potential intramolecular hydrogen bonding.

2. Results

2.1 Synthesis and Structure

The synthesis of the H_3t5a ligand was originally described using a synthetic strategy based on pyridazine ring contraction via electrochemical reduction.[25] The strategy consisted of a nine-step process with a 4% overall yield and the last electrochemical reduction step limited the synthesis to milligram scale. In this work, we prepare H_3t5a at a 1 g scale in 26% overall yield in a novel procedure (Scheme 1A). The 2-step synthesis involves a Stetter reaction [26,27] and a 1,4-diketone Paal-Knorr condensation followed by ester hydrolysis.

The H_3t5a ligand reacts with the Ru precursor, $\{Ru^{II}Cl_2(p\text{-cymene})\}_2$, in the presence of an excess of Et_3N to ensure deprotonation of the ligand (Scheme 1B). Subsequent addition of pyridine (py) generates a red octahedral complex $\{Ru^{II}(Ht5a\text{-}\kappa\text{-}N^2O)(py)_3\}$, $\mathbf{1}H^{II}(\kappa\text{-}N^2O)$, where the $Ht5a^{2-}$ ligand acts as tridentate meridional ligand with one of the pyridyl-carboxylate arms decoordinated. The monodentate pyridyl ligands occupy the other three positions as shown in the ORTEP plot depicted in Figure 1. Bonding distances and angles are unexceptional and similar to related Ru(II) complexes reported in the literature ($d_{Ru\text{-}O/Ru\text{-}N}$ = 1.9 - 2.1 Å).[28] Further, the ^{1}H NMR spectrum of $\mathbf{1}H^{II}(\kappa\text{-}N^2O)$ in methanol-d_4 confirms that the solid-state structure is maintained in solution (Figure 2).

Oxidation of complex $\mathbf{1}H^{II}(\kappa\text{-}N^2O)$ dissolved in water by air generates the green paramagnetic Ru^{III} complex $\{Ru^{III}(t5a\text{-}\kappa\text{-}N^3O^{1.5})(py)_2\}$, $\mathbf{2}^{III}(\kappa\text{-}N^3O^{1.5})$, where the pyridyl-carboxylate arm substitutes the initial equatorial pyridyl ligand as shown in the ORTEP plot in Figure 1. The coordination around the Ru metal center can be considered as 6.5 because one of the carboxylate Ru-O bonds is slightly elongated ($d_{Ru\text{-}O}$ = 2.31 Å) in respect to the usual Ru-N/Ru-O distances ($d_{Ru\text{-}O/Ru\text{-}N}$ = 1.9 - 2.1 Å). The structure and the elongated bond parallels that of Ru-tda in the III oxidation state reported earlier ($d_{Ru\text{-}N}$= 2.38 Å) and assigned as a half coordination to keep truck of the precise coordination environment.[12] Thus for the elongated bond distance or contact displayed in the X-ray structure we use the notation $\mathbf{2}^{III}(\kappa\text{-}N^3O^{1.5})$. Finally, the ^{1}H NMR spectrum of $\mathbf{2}^{III}(\kappa\text{-}N^3O^{1.5})$ in methanol-d_4 (Figure 2), shows two broad resonances in the 0-10 ppm window that reflects its paramagnetic electronic structure.

Addition of Ce^{IV} to a methanol solution of $\mathbf{2}^{III}(\kappa\text{-}N^3O^{1.5})$ generates the orange diamagnetic Ru^{IV} complex $\{Ru^{IV}(t5a\text{-}\kappa\text{-}N^3O^2)(py)_2\}^+$, $\{\mathbf{2}^{IV}(\kappa\text{-}N^3O^2)\}^+$, with a 7-coordinate Ru metal center. The $t5a^{3-}$ acts as a pentadentate ligand and generates a distorted pentagonal bipyramid geometry as can be observed in the ORTEP plot in Figure 1. We define the "outer equatorial angle" as the ORuO angle, that in this case is of approximately 72° in line with the pentagonal bipyramid geometry. Under this geometry, the d^4 Ru^{IV} ion is low spin and diamagnetic with fully occupied d_{xz} and d_{yz} orbitals.[29] The symmetry increase and high oxidation state of the complex results in a ^{1}H NMR spectrum where fewer resonances appear at lower fields with respect to the Ru^{II} parent complex. Finally, half a molecule of $\{Ce^{III}(CH_3OH)(NO_3)_5\}^{2-}$ compensates the positive charge of $\{\mathbf{2}^{IV}(\kappa\text{-}N^3O^2)\}^+$ as shown in the crystal structure (See Figure S30 in the Supporting Information (SI)).

DFT calculations at M06-L level of theory[30] provide optimized structures for complex $\mathbf{2}^{\mathbf{III}}(\kappa\text{-}N^3O^{1.5})$ and $\{\mathbf{2}^{\mathbf{IV}}(\kappa\text{-}N^3O^2)\}^+$ (see computational methods in the SI). The structure of $\{\mathbf{2}^{\mathbf{IV}}(\kappa\text{-}N^3O^2)\}^+$ shows a 7-coordinate complex that nicely agrees with the metric parameters of the XRD structure as shown in Table S1. However, the DFT optimized structure of $\mathbf{2}^{\mathbf{III}}$ also has a 6.5 coordination but with an elongated Ru-N pyridyl from the $t5a^{3-}$ ligand at 2.50 Å ($\kappa\text{-}N^{2.5}O^2$) instead of the carboxylate found in the crystal structure. Nevertheless, the relative energies of the two isomers, where $t5a^{3-}$ coordinates the Ru center in the $\kappa\text{-}N^{2.5}O^2$ and $\kappa\text{-}N^3O^{1.5}$ fashions, are likely to be very similar and thus both isomers might rapidly interconvert in solution. To probe this point further, we performed constrained optimizations to obtain the $\kappa\text{-}N^3O^{1.5}$ isomer and found very small energy difference between the two isomers (ΔE = 1.3 kcal/mol at M06 level of theory, $\kappa\text{-}N^3O^{1.5}$ being more stable than the $\kappa\text{-}N^{2.5}O^2$ coordination). For simplicity purposes, from now on we will use the label $\mathbf{2}^{\mathbf{III}}(\kappa\text{-}N^3O^{1.5})$ to refer to both of them. A similar phenomenon was experimentally observed for Ru-tda complex $\{\mathbf{3}^{\mathbf{III}}\}^+$, where the unit cell of its X-ray structure contained one molecule of the $\kappa\text{-}N^{2.5}O^2$ isomer and another one of the $\kappa\text{-}N^3O^{1.5}$ isomer.[12]

2.2 Redox Properties

We assess the electrochemical properties of the complexes described in this work by Cyclic Voltammetry (CV) and Differential Pulse Voltammetry (DPV). The electrochemical experiments are carried out in a typical three-electrode configuration using glassy carbon as the working electrode, Pt as the counter electrode and Hg/Hg_2SO_4 (MSE) as the reference electrode. All potentials in this work are reported versus NHE ($E_{NHE} = E_{MSE} + 0.65$ V).

Figure 3A shows the electrochemical behavior for $\mathbf{2}^{\mathbf{III}}(\kappa\text{-}N^3O^{1.5})$ analyzed by CV and DPV at *pH* = 7.0. The open circuit potential of $\mathbf{2}^{\mathbf{III}}(\kappa\text{-}N^3O^{1.5})$ appears at 0.35 V and is used as the starting potential of the CV. The potential is then scanned anodically to 1.15 V and back to -0.15 V where the scan direction is again changed to 0.70 V. A chemically reversible and electrochemically quasireversible ($\Delta E >$ 57 mV) wave appears at E^o_1 = 0.50 V (ΔE = 80 mV), which is associated with the reversible Ru^{IV}/Ru^{III} redox process. A second cathodic event occurs at lower potentials ($E_{c,p}$ = - 0.05 V) and is associated to the reduction from the Ru^{III} to the Ru^{II} state. The returning anodic wave appears at $E_{a,p}$ = 0.35 V with a large peak to peak separation (ΔE = 0.40 V*)* associated with the linkage isomerization outlined in the upper right part of Scheme 2. The square cycle is generated because 6.5 coordination is favored in the III oxidation state and disfavored at oxidation state II. In the latter, the pyridyl carboxylate arm decoordinates and the complex in the II oxidation states prefers 5.5-coordination. Further evidence for the presence of this square mechanism is obtained repeating the CV at faster scan rates both in MeOH and at *pH* = 7.0 where the cathodic wave of the $E^o_{2'}$ process can be observed (Figure S31-S32). This allows to calculate the III/II redox couple at *pH* = 7.0 that for $\mathbf{2}^{\mathbf{III}}(\kappa\text{-}N^{2.5}O)$ appears at $E_{2'}{}^o$ = 0.24 V (ΔE = 0.13 V). This value is consistent with the lower coordination number of the latter.

We attempted to compute the free energy of the 6.5-coordinate and 5.5-coordinate structures for the III and II oxidation states including explicit water molecules to account for hydrogen bonding interactions. The comparison of relative energies at M06 level of theory[31,32] indicates that 5.5-coordinate Ru-t5a complex is favored by 6.9 kcal/mol at oxidation state II. On the other hand, we could not obtain a fully optimized structure for 5.5-coordinate complex at III oxidation state as interconverts to the 6.5-coordinate isomer during geometry optimizations but we estimated the 5.5-coodinated complex to be ≈ 5 kcal/mol less stable compared to the 6.5-coordinate isomer (see Table S2 for the relative free energies and details). Overall, the computed energies support the proposed square mechanism.

To further spectroscopically characterize the species involved in this square cycle, we carried out a spectroelectrochemical experiment using an OTTLE cell for $\mathbf{2}^{\mathbf{III}}(\kappa\text{-}N^3O^{1.5})$.[33] Figure S33 shows the UV-vis spectral changes recorded every 19.5 mV for a CV experiment analogous to that of Figure 3A but at a scan rate of 2 mV/s. The UV-vis spectra exhibit isosbestic points in the Ru^{IV}/Ru^{III} and Ru^{III}/Ru^{II} reductive conversions while upon reaching the initial potential the spectrum is identical to the initial one, manifesting the reversibility of this transformation. This allows to obtain the UV-vis spectra for the dominating species at each oxidation stated namely, $\{\mathbf{2}^{\mathbf{IV}}(\kappa\text{-}N^3O^2)\}^+$, $\mathbf{2}^{\mathbf{III}}(\kappa\text{-}N^3O^{1.5})$ and $\mathbf{2}^{\mathbf{II}}(\kappa\text{-}N^{2.5}O)$.

The redox properties of complex $\mathbf{2}^{\mathbf{III}}(\kappa\text{-}N^3O^{1.5})$ were further analyzed at different *pHs* by CV and DPV. Figure 4 shows the derived Pourbaix diagram together with that of $\{Ru^{II}(tda\text{-}\kappa\text{-}N^3O)(py)_2\}$, $\mathbf{3}^{\mathbf{II}}$, for comparative purposes. The IV/III redox couple for both complexes is *pH* independent and is approximately 550 mV lower for the Ru-t5a complex. The extra negative charge of the $t5a^{3-}$ ligand clearly lowers the potential of the Ru^{IV}/Ru^{III} couple at the whole *pH* range as well as that of the Ru^{III}/Ru^{II} couple at *pH* > 5. Finally, the protonation of the dangling carboxylate of the $t5a^{3-}$ ligand results in the *pH* dependent process between *pH* = 1.0 and *pH* = 5.0 for the Ru^{III}/Ru^{II} couple, showing a slope of 60 mV/*pH*, with a pK_a = 5.0.

The ability of $\mathbf{2}^{\mathbf{III}}(\kappa\text{-}N^3O^{1.5})$ to act as precursor of a water oxidation catalyst was explored by scanning the potential up to 1.65 V at *pH* = 7.0. Figure 3B shows the presence of a large electrocatalytic current starting at 1.40 V associated with the generation of $\{\mathbf{2}^{\mathbf{V}}(\kappa\text{-}N^3O^2)\}^{2+}$. The latter exhibits fast water coordination and H^+ loss generating $\mathbf{2}^{\mathbf{V}}(O)(\kappa\text{-}N^2O)$, that is responsible for water oxidation catalysis (see left hand side of Scheme 2 and DFT below for the characterization of the active species at oxidation state V). The crossing at *E* = 1.35 V in the returning scan is attributed to the increase of the active catalyst species $\mathbf{2}^{\mathbf{V}}(O)(\kappa\text{-}N^2O)$ generated over the positive scanning process, while catalysis is occurring in parallel, together with the potential adsorption of the catalyst at the surface of the electrode as shown in Figure S37 in the SI. We performed an analogous experiment that cycled $\mathbf{2}^{\mathbf{III}}(\kappa\text{-}N^3O^{1.5})$ in the II, III and IV oxidation states (see Figure S40). The consecutive voltammograms showed unchanged response over the cycles, indicating that water coordination only occurs when $\mathbf{2}^{\mathbf{III}}(\kappa\text{-}N^3O^{1.5})$ reaches the V oxidation state.

Density functional theory (DFT) calculations at M06 level of theory were performed to assess the coordination of water to Ru-t5a and the relative stabilities of different protonation states and

isomers at different oxidation states (Figure S42-S47, Table S3-S12, Scheme S2-S7). At *pH* = 7.0, the coordination of a water molecule to the Ru^{IV}-t5a is uphill by 18.2 kcal/mol (see upper part of Scheme 2 and Table S10). In the V oxidation state, the free energy cost decreases to 5.0 or 12.7 kcal/mol respectively for $\mathbf{2}^{\mathbf{V}}$(O)(κ-$N^{2.5}$O) and $\mathbf{2}^{\mathbf{V}}$(O)(κ-N^2O) isomers (see lower part of Scheme 2). The decrease in free energy cost is consistent with the electrochemical results that show that water mainly coordinates at oxidation state V.

The optimized structures for both complexes, $\mathbf{2}^{\mathbf{V}}$(O)(κ-N^2O) and $\mathbf{2}^{\mathbf{V}}$(O)(κ-$N^{2.5}$O), are shown in Figure 5 and illustrate the different coordination subtleties of the pyridyl-carboxylate arm. For $\mathbf{2}^{\mathbf{V}}$(O)(κ-$N^{2.5}$O) the complex can be considered 6.5-coordinate with a Ru-N bond distance of 2.4 Å, whereas for $\mathbf{2}^{\mathbf{V}}$(O)(κ-N^2O) the same distance is 3.2 Å, and thus the complex is clearly 6-coordinate. The free energies for the 6.5-coordinate $\mathbf{2}^{\mathbf{V}}$(O)(κ-$N^{2.5}$O) and the 6-coordinate $\mathbf{2}^{\mathbf{V}}$(O)(κ-N^2O) only differ by 7.7 kcal/mol as indicated in Scheme 2 and thus at RT they probably interconvert very fast. For simplicity, in the description of the catalytic cycle we will only consider the 6-coordinate complex $\mathbf{2}^{\mathbf{V}}$(O)(κ-N^2O).

2.3 Water oxidation catalysis

In order to study the activity of the $\mathbf{2}^{\mathbf{V}}$(O)(κ-N^2O) catalyst, we carried out 50 repetitive CV scans as shown in Figure 3C. For this experiment, the potential was scanned up to 1.50 V to avoid the crossing point described in the previous section. In the CV, a progressive increase of current density is observed in the 1.25 V – 1.50 V region as the repetitive cycling proceeds consistent with the increased concentration of active species. In addition, new waves appear in the potential range 0.60 V - 0.95 V associated with the formation of reduced active species derived from $\mathbf{2}^{\mathbf{V}}$(O)(κ-N^2O) generating their corresponding Ru-aqua/hydroxo species whose potential structures were calculated based on DFT and are drawn in Scheme 3 and in the SI. At the end of the 50 cycles, the redox waves of the active catalyst $\mathbf{2}^{\mathbf{V}}$(O)(κ-N^2O) appear in the CV together with those of its precursor complex $\mathbf{2}^{\mathbf{V}}$(κ-N^3O^2), with which is in equilibrium in solution. The comparison of the first and the last cycle of the experiment also clearly indicates that this equilibrium only occurs when the complex reaches oxidation state V.

The *pH* dependency of the Ru^V/Ru^{IV} redox couple of complex $\mathbf{2}^{\mathbf{V}}$(O)(κ-N^2O) is reported in the SI (Figure S36) and a plot of its E^o vs *pH* in shown in Figure 4. As it can be seen in the Pourbaix diagram the pK_a of the Ru^{IV} couple (Ru^{IV}-OH -> Ru^{IV}-O + H^+) is 8.0 (pK_a^{calc} = 7.5). Thus, above *pH* = 8.0 the potential of the Ru^V/Ru^{IV} couple is *pH* independent whereas below *pH* 8.0 increases by approximately 60 mV per *pH* unit. The Ru^V-O analog $\{Ru^V(O)(tda{-}\kappa\text{-}N^3O)(py)_2\}^+$, $\{\mathbf{3}^{\mathbf{V}}(O)\}^+$, is also plotted in Figure 4B for comparison purposes. It is striking to see that the V/IV redox potential differs by less than 20 mV at the same *pH* given the sharp differences among the redox couples of their precursors, due to the different number of anionic donors of their equatorial ligands, $t5a^{3-}$ and tda^{2-}. A kinetic analysis was also carried out for $\mathbf{2}^{\mathbf{V}}$(O)(κ-N^2O) at *pH* = 7.0 based on Foot of the

Wave Analysis (FOWA) giving a calculated TOF_{MAX} of 9400 s^{-1} (Figure 3D). This value is in the same range of that exhibited by $\mathbf{3}^{\mathbf{V}}$(O).

An additional phenomenon that occurs during the electrocatalytic process at *pH* = 7.0 is the adsorption of reduced species of $\{\mathbf{2}^{\mathbf{V}}(\kappa\text{-}N^3O^2)\}^{2+}$ and $\mathbf{2}^{\mathbf{V}}$(O)(κ-N^2O) at the electrode surface. This is observed when placing the electrode used after catalysis in a clean electrolyte solution at the same *pH* and running again a CV (Figure S37). The CV of the electrode in a fresh solution show identical electrochemical events to those of $\{\mathbf{2}^{\mathbf{V}}(\kappa\text{-}N^3O^2)\}^{2+}$ and $\mathbf{2}^{\mathbf{V}}$(O)(κ-N^2O) in solution (see Figure S37). Therefore, the deposited material on the surface of the glassy carbon electrode consists of the molecular complexes $\{\mathbf{2}^{\mathbf{V}}(\kappa\text{-}N^3O^2)\}^{2+}$ and $\mathbf{2}^{\mathbf{V}}$(O)(κ-N^2O) adsorbed on the electrode surface. The adsorbed species account for roughly 25 % of the catalytic activity at *E* = 1.5 V in the CV. In sharp contrast, at *pH* = 1.0 the adsorbed species are responsible for practically all the catalytic activity at *E* = 1.75 V in the CV as can be observed in Figures S38-S39. The Foot of the Wave Analysis (FOWA) methodology calculates TOF_{MAX} at the onset of the water oxidation catalytic wave (*E* < 1.35 V, see Figure 3D) where the contribution of the adsorbed species is negligible (see Figure S37). The V/IV redox potential used in the FOWA methodology is extracted from DPV measurements, since it is obviously not possible to measure from simple cyclic voltammetry experiments. This is an approximation that we have previously discussed for related catalysts.[34]

We also studied the ability of the $\mathbf{2}^{\mathbf{V}}$(O)(κ-N^2O) catalyst to generate O_2 in the bulk in solution photochemically using a Hansateck® apparatus. The instrument measures the O_2 in solution and is performed in the absence of headspace. A solution (1.2 mL) containing $\mathbf{1}H^{\mathbf{II}}$($\kappa$-$N^2$O) (18 μM) a catalyst precursor, $[Ru(bpy)(bpy\text{-}COOMe)_2]^{2+}$ as a dye (0.1 mM) and $Na_2S_2O_8$ as sacrificial electron acceptor (10 mM) was irradiated for 20 minutes (see Figure S41 in the SI for further details). This generated 360 nmols of O_2 (16.7 TONs) that basically corresponds to the concentration of saturated O_2 in solution. The absence of headspace in Hansateck® apparatus makes the O_2 saturation the liming factor of the photocatalytic system. The performance exhibit by the Ru-t5a catalyst parallels to that of $\{Ru^V(O)(tda{-}\kappa\text{-}N^3O)(py)_2\}^+$, $\{\mathbf{3}^{\mathbf{V}}(O)\}^+$.[18] The nature of the catalyst was monitored by CV showing that the initial catalyst precursor is fully converted into the Ru-OH catalytic species.

2.4 The water oxidation catalytic cycle

DFT calculations at M06 level of theory were carried out to investigate the catalytic cycle starting from $\mathbf{2}H^{\mathbf{II}}(OH_2)$($\kappa$-$N^2$O) (Scheme 3). As shown in Scheme 3, one possible activation pathway is three consecutive proton-coupled electron transfer steps, which results in generation of the $\mathbf{2}^{\mathbf{V}}$(O) complex. Details on other possible activation pathways are available in the SI. We studied both the energetics of the 6-coordinate and 6.5-coordinate complexes in the V oxidation state to be involved in O-O bond formation *via* a Water Nucleophilic Attack (WNA) mechanism. Additionally, we studied the catalytic cycle starting from the complex in the VI oxidation state, complex $\{\mathbf{2}^{\mathbf{VI}}(O)(\kappa\text{-}N^{2.5}O)\}^+$, where the Ru^{VI} is used to display the formal oxidation state since the last oxidation occurs in the pyrrolato ligand due to its high electron density.

Scheme 3 shows the catalytic cycle starting from the 6-coordinate $\mathbf{2}^{\mathbf{V}}$(O)(κ-N^2O) complex computed at *pH* = 0.0 and the analogous catalytic cycle starting from the 6.5-coordinate $\mathbf{2}^{\mathbf{V}}$(O)(κ-$N^{2.5}$O) and $\mathbf{2}^{\mathbf{VI}}$(O)(κ-$N^{2.5}$O) can be found in Scheme S3. The optimized transition state structures in the three cases consist of a water molecule interacting with the Ru=O moiety while the dangling carboxylate assists the proton transfer (Figure 5C and Figure S47). Among the three cases, the lowest activation free energy ($\Delta G^{\ddagger}$) is of 14.2 kcal/mol and it is displayed by the 6-coordinate complex $\mathbf{2}^{\mathbf{V}}$(O)(κ-N^2O) to yield to the 6-coordinate TS structure. Preserving 6.5-coordination in the O-O bond formation transition state requires an additional water molecule and is energetically unfavorable by ≈10 kcal/mol (Figure S47). In all cases, the products of the WNA steps are the hydroperoxo complexes that are further oxidized to the superoxo complexes. The water oxidation catalysis exhibited by complex $\mathbf{2}^{\mathbf{V}}$(O)(κ-$N^{2.5}$O) involves the coordination of a water to the Ru center upon the release of O_2. We performed constrained optimizations to examine the oxygen evolution step and estimated an activation energy of about 11 kcal/mol (Figure S48) so that the WNA is predicted to be the rate limiting chemical step for the catalytic cycle. Consequently, the liberation of O_2 and coordination of a water molecule yields the initial complex in the II oxidation state, complex $\mathbf{2}H^{\mathbf{II}}(OH_2)$(κ-$N^2$O) (Scheme 3 and Scheme S3). The $\mathbf{2}^{\mathbf{V}}$(O)(κ-$N^{2.5}$O) complex is 7.7 kcal/mol more stable than $\mathbf{2}^{\mathbf{V}}$(O)(κ-N^2O) so that there will be competition between WNA pathway of $\mathbf{2}^{\mathbf{V}}$(O)(κ-N^2O) and isomerization to $\mathbf{2}^{\mathbf{V}}$(O)(κ-$N^{2.5}$O). It is worth noting that the computed potential for oxidation of $\mathbf{2}^{\mathbf{V}}$(O)(κ-$N^{2.5}$O) to $\mathbf{2}^{\mathbf{VI}}$(O)(κ-$N^{2.5}$O) is only 1.26 V vs NHE. Furthermore, the WNA attack to this species has a $\Delta G^{\ddagger}$ = 18.1 kcal/mol and thus can be competing with the previous species at oxidation state V.

We also computed redox potentials for the processes in the catalytic cycle, which are summarized in Scheme 3. Among them, that associated with the Ru^{V}=O/Ru^{IV}-OH redox couple is the highest of the catalytic cycle. The computed potential is E_{calc} = 1.65 V at *pH* = 0.0, which is in agreement with the value extrapolated from the experimental Pourbaix diagram in Figure 4 (E_{exp} = 1.88 V).

3. Discussion

Seven-coordinate Ru complexes such as {Ru^{V}(O)(bda)(Me-py)$_2$}$^+$, {$\mathbf{5}^{\mathbf{V}}$(O)}$^+$, and {Ru^{V}(O)(tda-κ-N^3O)(py)$_2$}$^+$, {$\mathbf{3}^{\mathbf{V}}$(O)}$^+$, are receiving a great deal of attention because they are among the fastest and more rugged water oxidation catalysts described today. The latter at *pH* = 10.0 reaches TOF_{max} of 50.000 s^{-1} that is the fastest WOC ever reported and is actually two orders of magnitude faster than the OEC-PSII that turns at the millisecond time scale.[35,36] A question that arises here is if seven coordination is essential for Ru complexes in order to obtain fast water oxidation catalysis. For [Ru^{II}(bda)(Me-py)$_2$], $\mathbf{5}^{\mathbf{II}}$, and {Ru^{II}(tda-κ-N^3O)(py)$_2$}, $\mathbf{3}^{\mathbf{II}}$, seven coordination was achieved thanks to the presence of tetra- and pentadentate ligands respectively that coordinate at the equatorial positions of the Ru metal center. The constrained geometry of these ligands produce large "outer equatorial angles" O-Ru-X (X = O or N) of 123° and 122° respectively, that gives room for a seven coordination upon reaching oxidation states IV and above.

In the present work, we report the rich chemistry of a family of related Ru complexes containing the pentadentate adaptative ligand H_3t5a that can potentially loose up to three protons. The t5a^{3-} ligand is similar to the tda^{2-} but replacing the central pyridyl ring by a pyrrolyl group (see Scheme 1 for a drawing). This produces two major changes in coordination properties of this ligand. First, it is a much powerful electron donating ligand since it can act as a trianionic ligand as opposed to the maximum dianonic capacity of tda^{2-} and secondly the five member pyrrolyl ring generates $CCN_{pyrrolyl}$ angles 6 degrees larger than $CCN_{pyridyl}$ (See Chart 1). This will further increase the equatorial constrain of the ligand by further opening up the "outer equatorial angles". This can be nicely observed by comparing this angle in the X-ray structure of [Ru(tda)(py)(dmso)] that is of 123º with that of the DFT calculated structure {Ru^{II}(t5a-κ-N$^{2.5}$O)(py)$_2$}, that increase up to 135º.

These electronic and geometrical particularities influence the coordination structure and reactivity both a low oxidation states (II and III) and at high oxidation states (IV and V).

3.1 Low oxidation states chemistry and linkage isomerism

At oxidation state III, DFT calculations suggest the presence of two isomers for the non-aqua type of species, **2**^{III}(κ-N^{3}O$^{1.5}$) and **2**^{III}(κ-N$^{2.5}$O^2), with relatively similar energies. These isomers have the same coordination number and closely related structures where the Ru metal center can easily glide in the equatorial plane within the coordination framework established by the coordinating atoms of the t5a^{3-} ligand, accessing two limiting geometrical positions at κ-N^{3}O$^{1.5}$ and κ-N$^{2.5}$O^2, as a consequence of the ligand flexibility.

At oxidation state II, a 5.5 coordination complex **2**^{II}(κ-N$^{2.5}$O), is found as the most stable isomer that is quite remarkable for a d^6 low spin Ru(II) center, that is generally six coordinated with an octahedral type of geometry. The 5.5 coordination, not found in the related Ru-tda complexes, is a consequence of the equatorial nature of the coordinating atoms of the t5a^{3-} ligand together with the additional geometrical constrains due to the 6 degrees larger $CCN_{pyrrolyl}$ angles imposed by the pyrrolyl groups as compared to the pyridyl one.

This peculiar ligand geometry and flexibility is also responsible for the linkage isomerism found within oxidation states II and III displayed in the right upper part of Scheme 2, that is not observed for related non-aqua Ru-tda complexes. On the other hand, the trianionic character of the ligand is manifested in a large cathodic shift of approximately 600 mV for the III/II couple of **2**^{III}(κ-N^{3}O$^{1.5}$) as compared to that of {Ru^{III}(tda-κ-N^{3}O$^{1.5}$)(py)$_2$}$^+$, **3**^{III}(κ-N^{3}O$^{1.5}$) where the tda^{2-} ligand is dianionic.

3.2 High oxidation states chemistry and implications for water oxidation catalysis.

At oxidation state IV both the X-ray structure and DFT calculations for {**2**^{IV}(κ-N^{3}O^2)}$^+$, display a seven coordinated Ru center with a pentagonal bipyramid geometry, expected for a d^4 ion with the t5a^{3-} favoring this geometry at the equatorial plane. The electronic influence of an additional

charge is manifested again by a 500 mV cathodic shift upon comparing the IV/III redox couple of $\{\mathbf{2}^{\mathbf{IV}}(\kappa\text{-}N^3O^2)\}^{+}$ with regard to that of $\{\mathbf{3}^{\mathbf{IV}}(\kappa\text{-}N^3O^2)\}^{2+}$ (See Pourbaix diagram in Figure 4).

In sharp contrast, for the aquated species at oxidation state V a coordination environment of 6.5 and 6 has been proposed based on DFT calculations for species $\mathbf{2}^{\mathbf{V}}(O)(\kappa\text{-}N^{2.5}O)$ and $\mathbf{2}^{\mathbf{V}}(O)(\kappa\text{-}N^2O)$, respectively. The energy of these species only differs in 7.7 kcal/mol and thus in solution they are expected to interconvert very fast, thus manifesting again the adaptative capacity of the $t5a^{3-}$ ligand. The loss of the seventh coordination position renders complex $\mathbf{2}^{\mathbf{V}}(O)(\kappa\text{-}N^2O)$ the perfect catalyst to analyze the role of the seventh coordination in the two of the benchmarking parameters of the water oxidation catalysis: the potential of the V/IV redox couple (the overpotential) and the rate of the catalysis.

The 6-6.5 coordination number of $\mathbf{2}^{\mathbf{V}}(O)(\kappa\text{-}N^2O)$ and $\mathbf{2}^{\mathbf{V}}(O)(\kappa\text{-}N^{2.5}O)$ species is consistent with the potential of the V/IV redox couple shown in the Pourbaix diagram (Figure 4, red line). In this regard, we have recently uncovered a correlation between the E^o (Ru^{V}=O/Ru^{IV}=O) and the coordination number of the Ru center together with the number of negative charges, for a series of water oxidation catalysts. Table 1 gathers selected electrochemical and electronic properties of complex $\mathbf{2}^{\mathbf{V}}(O)(\kappa\text{-}N^2O)$ together with those of related water oxidation catalysts already described in the literature for comparison purposes. The $E^o_{(RuV=O/RuIV=O)}$ for $\mathbf{2}^{\mathbf{V}}(O)(\kappa\text{-}N^2O)$ is 1.41 V, that aligns very well with the other 6-coordinate complexes containing two anionic charges such as $\{Ru^{V}(O)(pdc)(Me\text{-}py)_2\}^{+}$, $\{\mathbf{7}^{V}(O)\}^{+}$ that has a $E^o_{(RuV=O/RuIV=O)}$ = 1.35 V (See Table 1; pdc^{2-} is 2,6-dicarboxylatopyrine).[23,37,38] Therefore, the loss of the seven coordination causes the increase of the potential of Ru^{V}=O/Ru^{IV}=O redox couple by at least 200 mV.[23]

The lower coordination number for $\mathbf{2}^{\mathbf{V}}(O)(\kappa\text{-}N^2O)$ with regard to that of $\{\mathbf{3}^{\mathbf{V}}(O)(\kappa\text{-}N^3O)\}^{+}$, is a consequence of mainly two factors. First a geometric effect related to the 2 x 6 ° = 12° $CCN_{pyrrolyl}$ angles that largely increases the "outer coordination angle" at the equatorial zone described above and secondly the large electron density transmitted to the Ru center via the pyrrolato and carboxylato groups. The latter already transmit a large degree of electron density to the metal center and thus an additional coordination is not crucial to stabilize the putative oxidation state V for this complex.

From a mechanistic perspective the O-O bond formation occurs at oxidation state V as proposed in Scheme 3 and evidenced by the electrocatalytic phenomena observed in Figure 3 and Figure S41. At this stage the transition state structure shown in Figure 5C, shows the key role of the dangling carboxylate as an intramolecular proton acceptor. This decreases the energies of activation of the rds to 14.2 kcal/mol and ensures fast catalysis. Indeed we calculate a TOF_{max} of 9400 s^{-1}, which is among the highest reported in the literature at pH = 7.0,[12,39,40] including those exhibited by Ru-tda complexes.[12] The key role of the intramolecular H bonding is consistent with recent combined experimental-computational works that indicate that the rate of the water oxidation reaction increases by 3-4 orders of magnitude thanks to strategically situated pendant base.[23] Here it is interesting to notice that the fast rate in the catalysis occurs besides the loss of the seven coordination by $\mathbf{2}^{\mathbf{V}}(O)(\kappa\text{-}N^2O)$.

4. Conclusions

In conclusion, we report the detailed characterization of the spectroscopic, electrochemical and catalytic properties of a family of Ru complexes containing the adaptative t5a^{3-} ligand, nicely complemented with DFT calculations. This work manifests how subtle changes on ligand geometry, the 12^{o} effect, can exert dramatic effects on complex geometry and reactivity. In particular, it highlights the interplay between coordination number 6 and 7 at different oxidation states, the degree of anionic character of the ligand, and the crucial role of the terminal carboxylate strategically situated close to the Ru-OH moiety can act as both H-bonding site and proton acceptor.

The present work reveals that for the design of fast water oxidation catalysts that contain ligands that are highly anionic and that sufficiently reduce the redox potential of the V/IV couple, the seven coordination is actually not needed provided the ligand design is such that it offers the means of an intramolecular proton transfer at the O-O bond formation step. On the other hand, for ligands that have less electron donating capacity the seven coordination will be crucial to be able to achieve oxidation state V at a relatively low potential.

5. Acknowledgments

R.M., AL and XS acknowledge MINECO and FEDER (CTQ2016-80058-R, CTQ2015-64261-R, SEV 2013-0319, ENE2016-82025-REDT, CTQ2016-81923-REDC), AGAUR (2014-SGR-915) and “La Caixa” foundation. The work carried out at Brookhaven National Laboratory (M.Z.E.) was supported by the U.S. Department of Energy, Office of Science, Division of Chemical Sciences, Geosciences, & Biosciences, Office of Basic Energy Sciences under contract DE-SC0012704. The ligand synthesis of this project was implemented by CHEM-Symbiose, a technological platform devoted to the synthesis of molecules. The authors are very grateful to the core facility networks Biogenouest (Network of Technological Platform) and IBISA (Infrastructures en Biologie Sante et Agronomie) for their support.

6. Associated Content

The Supporting Information (SI) is available free of charge via the Internet at http://pubs.acs.org. Experimental details as well as additional spectroscopic, electrochemical, and crystallographic results and DFT data (PDF) and X-ray data (CIF)

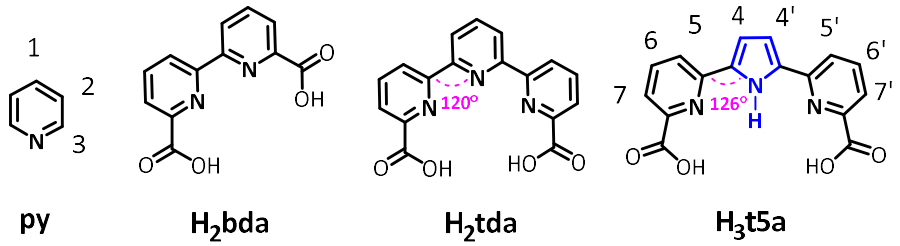

Chart 1: Ligands used and discussed in this work together with labeling and numbering.

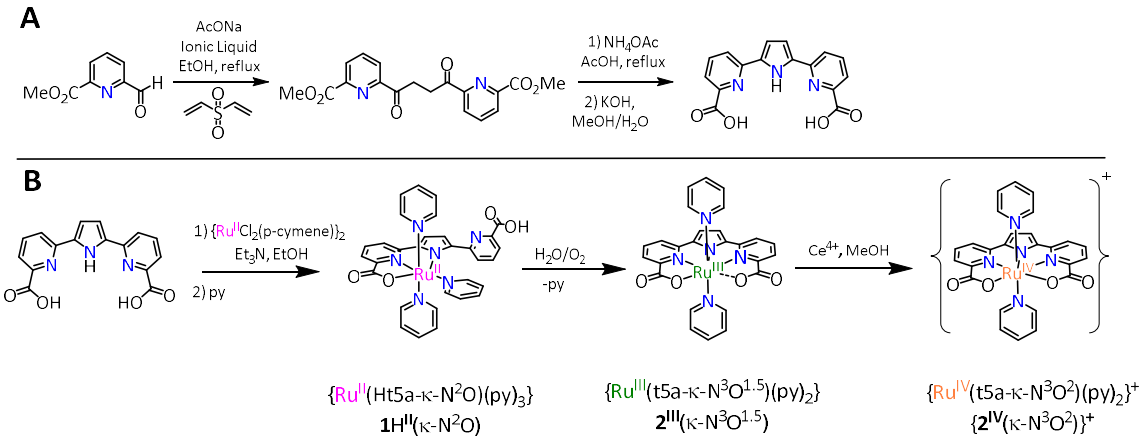

Scheme 1: Synthetic route for the preparation of H_3t5a ligand (**A**) and $\mathbf{1}H^{II}(\kappa\text{-}N^2O)$, $\mathbf{2}^{III}(\kappa\text{-}N^3O^{1.5})$ and $\{\mathbf{2}^{IV}(\kappa\text{-}N^3O^2)\}^+$ complexes (**B**). Dashed lines indicate contacts ($d_{Ru\text{-}O/Ru\text{-}N}$ = 2.3-2.8 Å).

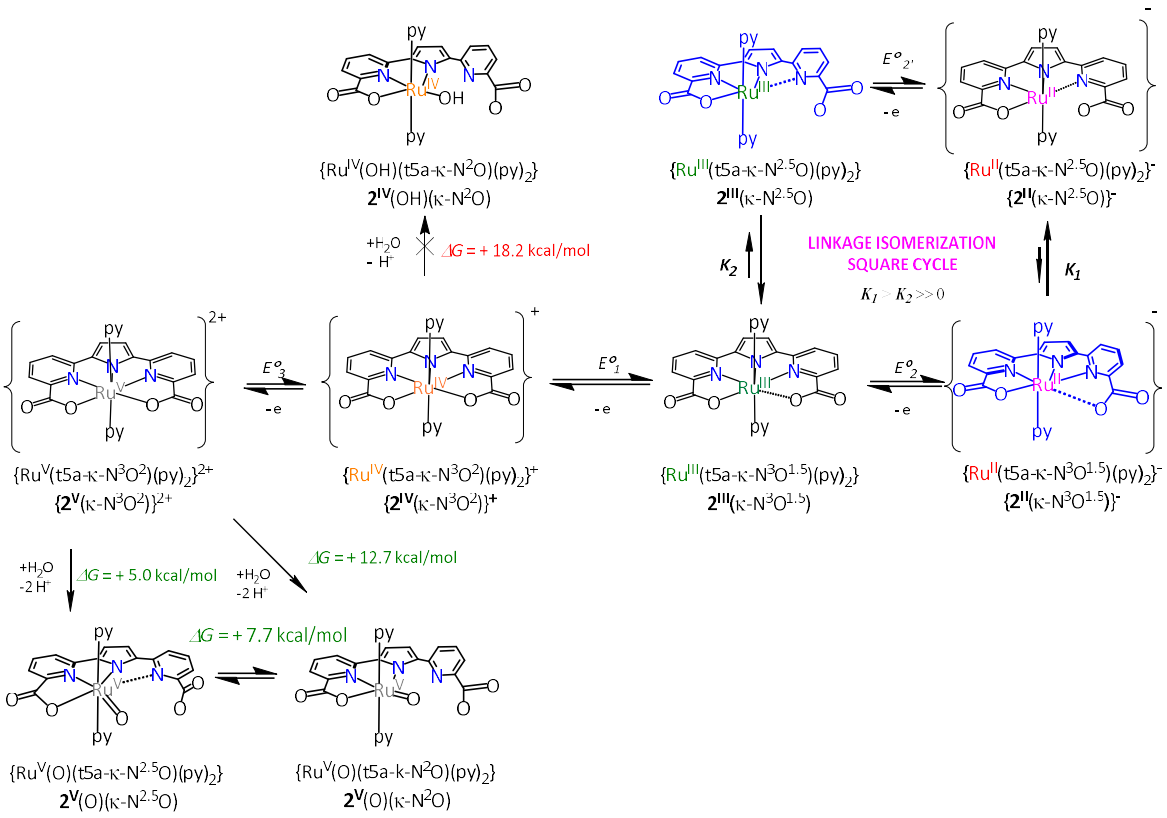

Scheme 2: Redox processes related to complex **2**^{III}(κ-N^{3}O$^{1.5}$) together with the generation of catalyst **2**^{V}(O)(κ-N^{2}O)**.** Blue colored species undergo fast isomerization in the square cycle. The free energy changes (ΔG) are at M06 level of theory at *pH* = 7.0. Dashed lines indicate contacts ($d_{Ru\text{-}O/Ru\text{-}N}$ = 2.3-2.8 Å).

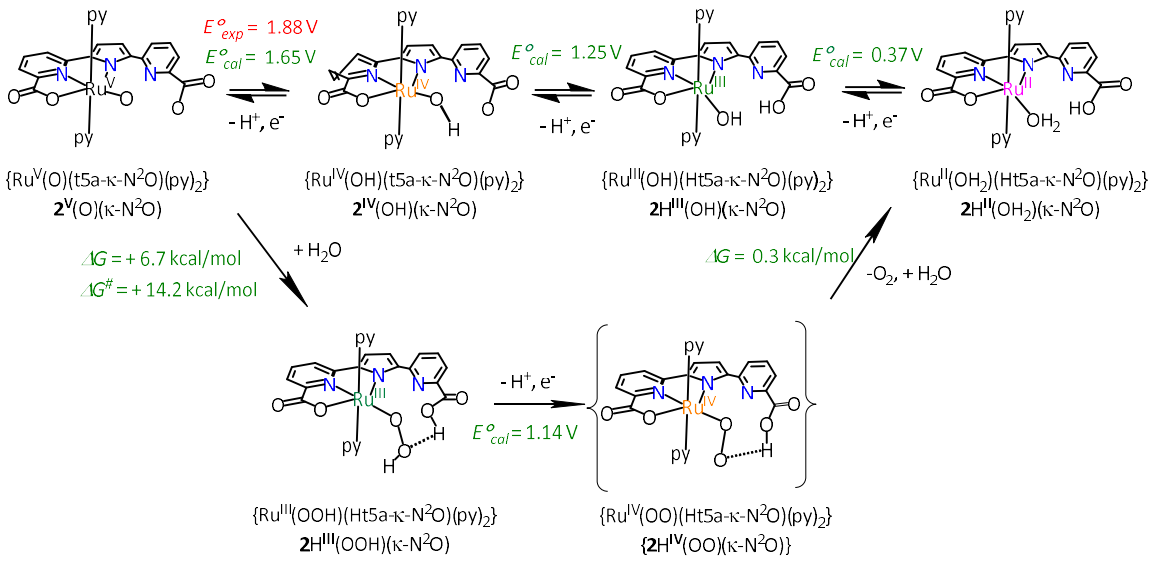

Scheme 3: Schematic representation of Ru-aqua species together with key intermediates and reactions in the catalytic water oxidation mechanism exhibited by complex $\mathbf{2}^{\mathbf{V}}$(O)(κ-N^2O) at *pH* = 0.0.

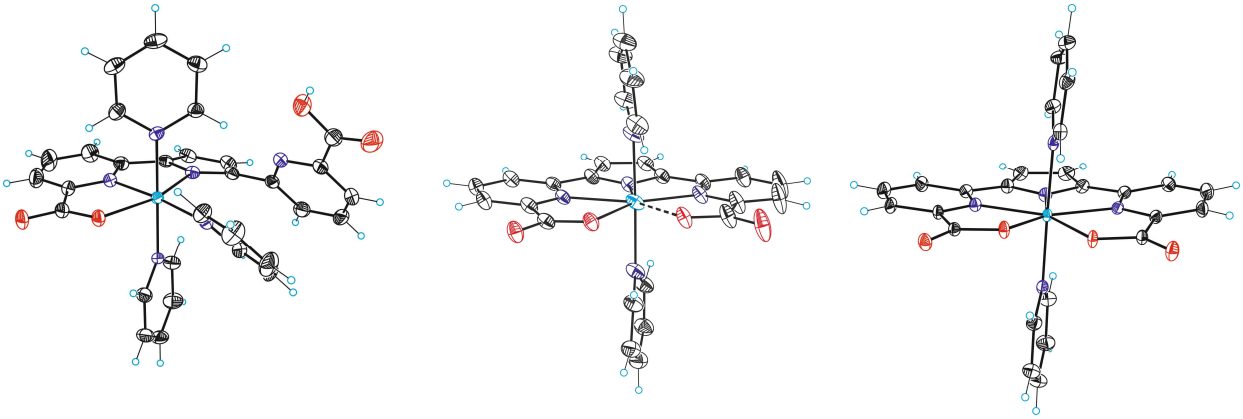

Figure 1: ORTEP plot (ellipsoids 50% of probability) of complexes **1**H^{II}(κ-N^2O) (left), **2**^{III}(κ-$N^3O^{1.5}$) (middle) and {**2**^{IV}(κ-N^3O^2)}$^+$ (right). Color codes: Ru, cyan; N, blue; O, red; C, black and H; white. See Table S1 for the distances. Dashed lines indicate contacts ($d_{Ru\text{-}O/Ru\text{-}N}$ = 2.3-2.8 Å).

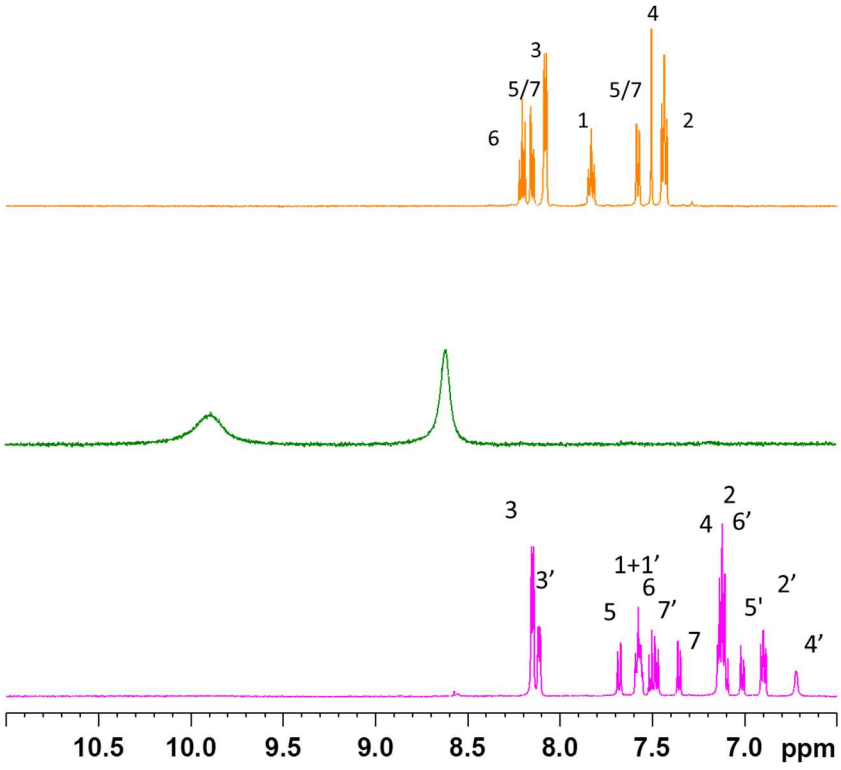

Figure 2: ^{1}H NMR of complexes **1**H^{II}(κ-N^2O) (pink), **2**^{III}(κ-$N^3O^{1.5}$) (green) and {**2**^{IV}(κ-N^3O^2)}$^+$ (orange) in methanol-d_4. See Chart 1 for the numbering.

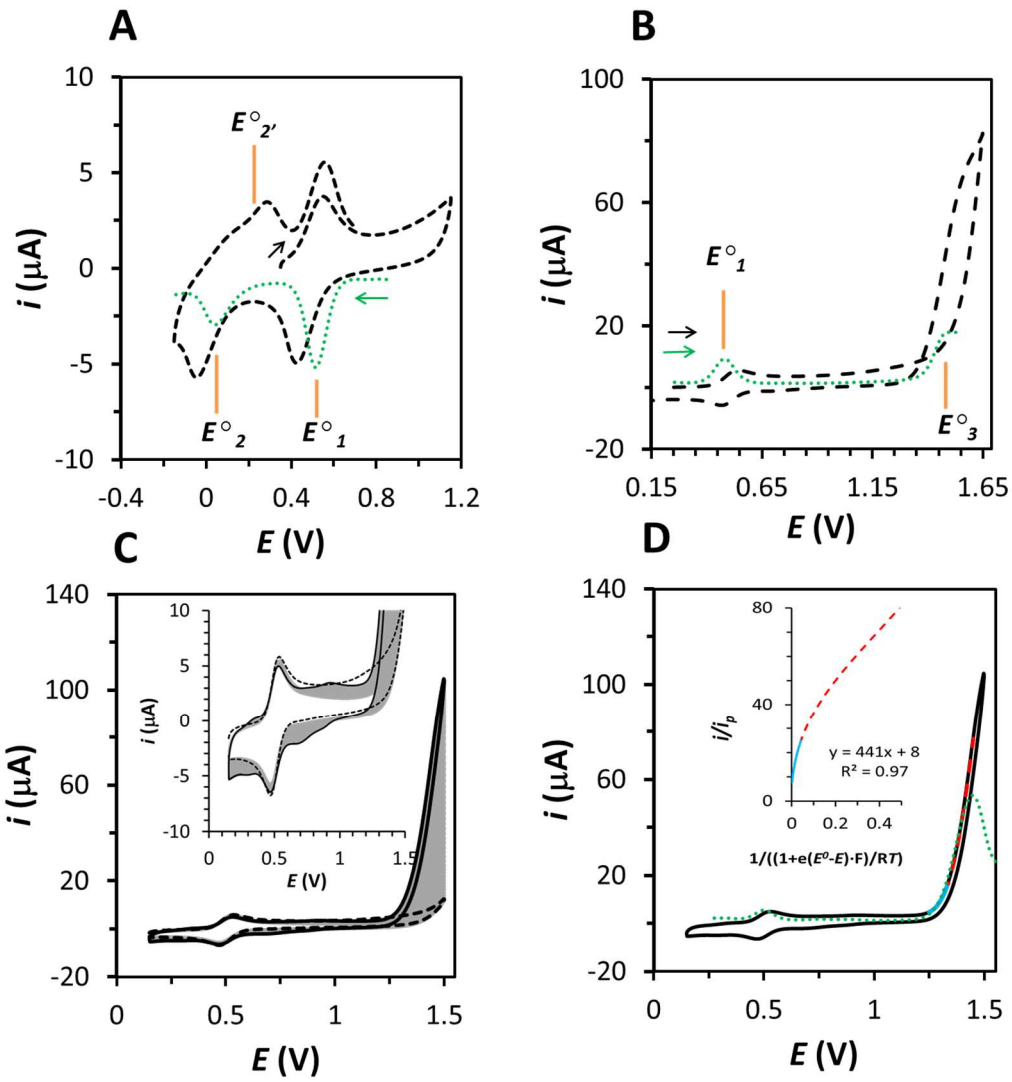

Figure 3: **A** and **B,** CV experiments (black dashed line) and DPVs experiments (green pointed line) of 0.5 mM $\mathbf{2}^{\mathbf{III}}(\kappa\text{-}N^3O^{1.5})$ at *pH* = 7.0. Arrows indicate initial potential and scan direction for CV (black line) and DPV (green line). The orange lines indicate the E^o associated with the different redox couples outlined in Scheme 2. Measurements were done under N_2 and the scan rate was 0.1 V/s. **C**, 50-repetitive CV experiment of $\mathbf{2}^{\mathbf{III}}(\kappa\text{-}N^3O^{1.5})$ (0.5 mM) at *pH* = 7.0 (dashed black line is the first cycle, solid black line is the 50th cycle and grey lines are the cycles in between). The inset shows an enlargement between -10 μA and 10 μA. The scan rate was 0.1 V/s. See electrochemcial methods in the SI for further details. **D**, 50th CV cycle (black solid line) and DPV experiment (green pointed line) of a mixture containing complex $\{\mathbf{2}^{\mathbf{IV}}(\kappa\text{-}N^3O^2)\}^+$ and complex $\mathbf{2}^{\mathbf{V}}(O)(\kappa\text{-}N^2O)$ (black solid line) together with the Foot of the Wave Analysis (FOWA) of complex $\mathbf{2}^{\mathbf{V}}(O)(\kappa\text{-}N^2O)$. The points used for FOWA are in the red dashed line and the points used for the lineal fit are cyan. $\mathbf{TOF_{MAX}}$ = 9400 s^{-1} was extracted from the analysis using E^o extracted from DPV (E^o = 1.44 V). See Figure S37 for a CV of the bare electrode together with CV of the electrode after the 50th cycles.

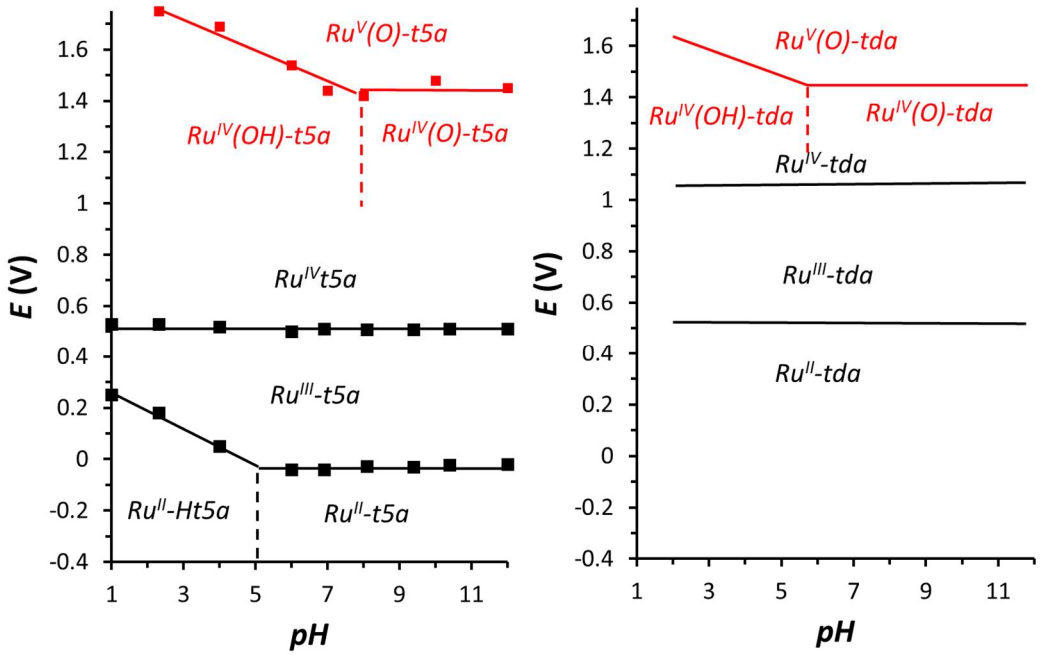

Figure 4: Left, Pourbaix diagram for $\mathbf{2}^{\mathbf{III}}$(κ-$N^3O^{1.5}$) (black dots and black solid lines) and for the Ru^V/Ru^{IV} redox couple of complex $\mathbf{2}^{\mathbf{IV}}$(OH)(κ-N^2O) (red dots and red solid lines). Both slopes for the *pH* dependent processes are circa 59 mV/*pH*. Right, Pourbaix diagram for $\{Ru^{IV}(tda\text{-}\kappa\text{-}N^3O^2)(py)_2\}^{2+}$, $\{\mathbf{3}^{IV}\}^{2+}$ (black solid line) and for the Ru^V/Ru^{IV} redox couple of $\{Ru^V(O)(tda\text{-}\kappa\text{-}N^3O)(py)_2\}^{+}$, $\{\mathbf{3}^{\mathbf{V}}(O)\}^{+}$, taken from the literature,[12] (red solid line). The overpotential (η) of the $\mathbf{2}^{\mathbf{V}}$(O)(κ-N^2O) catalyst towards water oxidation in the pH 2.0-8.0 region is η = 610 mV. This is the difference between the redox potential of the Ru^V/Ru^{IV} couple responsible for the electrocatalytic wave and the thermodynamic potential for the four electron oxidation of water.

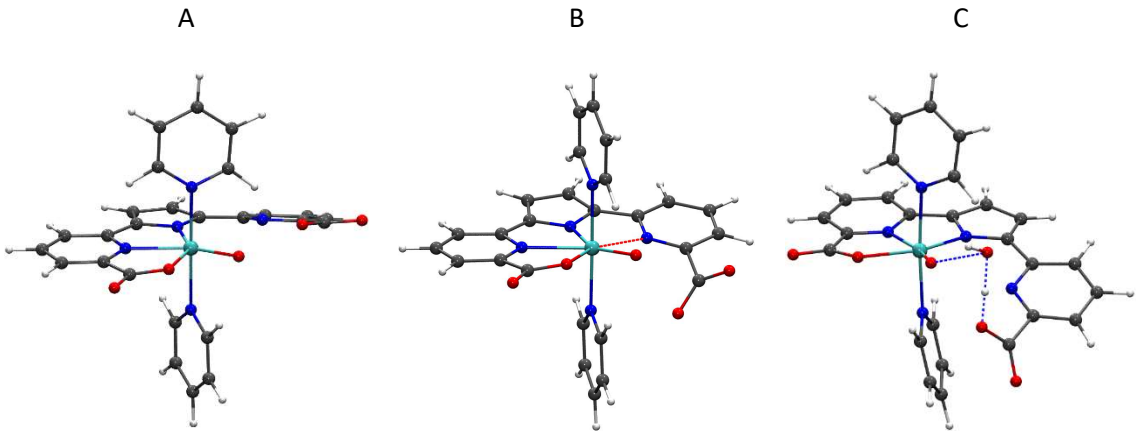

Figure 5: Optimized structures for $\{Ru^{V}(O)(t5a\text{-}\kappa\text{-}N^{2}O)(py)_2\}$, (A), $\{Ru^{V}(O)(t5a\text{-}\kappa\text{-}N^{2.5}O)(py)_2\}$, (B), and structure associated with the transition state $\{Ru^{V}(O)(t5a\text{-}\kappa\text{-}N^{2}O)(py)_2\}$ + H_2O, (C) at M06-L level of theory. Blue dashed lines indicate breaking and forming bonds in the TS. Red dashed lines indicate contacts ($d_{Ru\text{-}O/Ru\text{-}N}$ = 2.3-2.8 Å). Color code: Ru, turquoise; C, gray; N, blue; O, red; H, white.

Table 1: Selected redox potentials and pK_a values for complex **2**^{V}(O)(κ-N^{2}O) and related complexes previously described in the literature.

	7-coordinate Ru^{V}-O			**6-coordinate Ru^{V}-O**		
	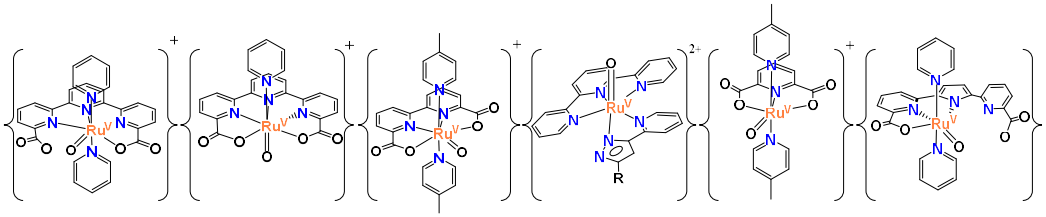					
Complex	{Ru^{V}(O)(tda-κ-N^{3}O)(py)$_2$}$^{+}$ {**3**^{V}(O)}$^{+}$	{Ru^{V}(O)(tda-κ-N^{3}O^2)(py)}$^{+}$ {**4**^{V}(O)}$^{+}$	{Ru^{V}(O)(bda)(Me-py)$_2$}$^{+}$ {**5**^{V}(O}$^{+}$	[b]{Ru^{V}(O)(trpy)(ppc)}$^{2+}$ {**6**^{V}(O)}$^{2+}$	[c]{Ru^{V}(O)(pdc)(Me-py)$_2$}$^{+}$ {**7**^{V}(O)}$^{+}$	{Ru^{V}(O)(t5a-κ-N^{2}O)(py)$_2$} {**2**^{V}(O)(κ-N^{2}O)}
[a]n^{-}	1	2	2	1	2	2
E^{o} (V) *Ru^{V}=O/Ru^{IV}=O*[d]	1.43	1.12	1.12	1.59	1.35	1.41
Ref.	12	23	17	37	38	this work

[a] negative charges given by the first coordination sphere excluding oxo/hydroxo groups.
[b] Hppc = ethyl 3-(pyridin-2-yl)-1H-pyrazole-5-carboxylate
[c] H_2pdc = pyridine-2,6-dicarboxylic acid
[d] redox potentials *vs*. NHE.

7. References

[1] Lewis, N. S. *Science* **2016**, *351*, 19201-19209.
[2] McKone, J. R.; Lewis, N. S.; Gray, H. B. *Chem. Mat.* **2014**, *26*, 407-414.
[3] Montoya, J. H.; Seitz, L. C.; Chakthranont, P.; Vojvodic, A.; Jaramillo, T. F.; Norskov, J. K. *Nat. Mater.* **2017**, *16*, 70-81.
[4] Helm, M. L.; Stewart, M. P.; Bullock, R. M.; DuBois, M. R.; DuBois, D. L. *Science* **2011**, *333*, 863-866.
[5] Costentin, C.; Drouet, S.; Robert, M.; Savéant, J.-M. *Science* **2012**, *338*, 90-94.
[6] Anderson, J. S.; Rittle, J.; Peters, J. C. *Nature* **2013**, *501*, 84-87.
[7] McCrory, C. C. L.; Jung, S.; Ferrer, I. M.; Chatman, S. M.; Peters, J. C.; Jaramillo, T. F. *J. Am. Chem. Soc*. **2015**, *137*, 4347-4357.
[8] Blakemore, J. D.; Crabtree, R. H.; Brudvig, G. W. *Chem. Rev.* **2015**, *115*, 12974-13005.
[9] Singh, A.; Spiccia, L. *Coord. Chem. Rev.* **2013**, *257*, 2607-2622.
[10] Garrido-Barros, P.; Gimbert-Suriñach, C.; Matheu, R.; Sala, X.; Llobet, A. *Chem. Soc. Rev.* **2017**, *46*, 6088-6098.
[11] Concepcion, J. J.; Tsai, M. K.; Muckerman, J. T.; Meyer, T. J. *J. Am. Chem. Soc.* **2010,** *132*, 1545-1557.
[12] Matheu, R.; Ertem, M. Z.; Benet-Buchholz, J.; Coronado, E.; Batista, V. S.; Sala, X.; Llobet, A. *J. Am. Chem. Soc.* **2015**, *137,* 10786-10795.
[13] Schulze, M.; Kunz, V.; Frischmann, P. D.; Würthner, F. *Nat. Chem.* **2016***, 8,* 576-583.
[14] Gersten, S. W.; Samuels, G. J.; Meyer, T. J. *J. Am. Chem. Soc.* **1982**, *104*, 4029–4030.
[15] Wasylenko, D. W.; Ganesamoorthy, C.; Henderson, M.; Koivisto, B. D.; Osthoff, H.; Berlinguette, C. P. *J. Am. Chem. Soc*. **2010**, *132*, 16094-16106.
[16] Polyansky, D. E.; Muckerman, J. T.; Rochford, J.; Zong, R.; Thummel, R. P.; Fujita, E. *J. Am. Chem. Soc.* **2011**, *133*, 14649-14665.
[17] Duan, L.; Bozoglian, F.; Mandal, S.; Stewart, B.; Privalov, T.; Llobet, A.; Sun, L. *Nat. Chem.* **2012,** *4,* 418-423.
[18] Francas, L.; Matheu, R.; Pastor, E.; Reynal, A.; Berardi, S.; Sala, X.; Llobet, A.; Durrant, J. R. *ACS Catal.* **2017**, *7*, 5142-5150.
[19] Duan, L.; Fischer, A.; Xu, Y.; Sun, L. *J. Am. Chem. Soc.* **2009**, *131*, 10397-10399.
[20] Richmond, C. J.; Matheu, R.; Poater, A.; Falivene, L.; Benet-Buchholz, J.; Sala, X.; Cavallo, L.; Llobet, A. *Chem. Eur. J.* **2014**, *20*, 17282-17286.
[21] Suga, M.; Akita, F.; Hirata, K.; Ueno, G.; Murakami, H.; Nakajima, Y.; Shimizu, T.; Yamashita, K.; Yamamoto, M.; Ago, H.; Shen, J.-R. *Nature* **2015**, *517*, 99-103.
[22] Xie, Y.; Shaffer, D. W.; Lewandowska-Andralojc, A.; Szalda, D. J.; Concepcion, J. J. *Angew. Chem. Int. Ed.* **2016**, *55*, 8067-8071.
[23] Matheu, R.; Ertem, M.; Gimbert-Suriñach, C.; Benet-Buchholz, J.; Sala, X.; Llobet *ACS Catal*. **2017**, *7,* 6525–6532.
[24] Kaveevivitchai, N.; Kohler, L.; Zong, R.; El Ojaimi, M.; Mehta, N.; Thummel, R. P. *Inorg. Chem.* **2013**, *52*, 10615-10622.
[25] Lautrette G.; Aube, C.; Ferrand, Y.; Pipelier, M.; Blot, V.; Kauffmann, B.; Dubreuil, D.; Huc, I. *Chem. Eur. J.* **2014**, *20*, 1547-1553.
[26] Stetter, H. *Angew. Chem. Int. Ed.* **1976**, *15*, 639–647.
[27] Imler, G. H.; Lu, Z.; Kistler, K. A.; Carroll, P. J.; Wayland, B. B.; Zdilla, M. J. *Inorg. Chem.* **2012**, *51*, 10122–10128.

[28] Richmond, C. J.; Matheu, R.; Poater, A.; Falivene, L.; Benet-Buchholz, J.; Sala, X.; Cavallo, L.; Llobet, A. *Chem. Eur. J.* **2014**, *20*, 17282-17286.
[29] Ohzu, S.; Ishizuka, T.; Hirai, Y.; Jiang, H.; Sakaguchi, M.; Ogura, T.; Fukuzumi, S.; Kojima, T. *Chem. Sci.* **2012**, *3*, 3421-3431.
[30] Zhao, Y.; Truhlar, D. G. *J. Chem. Phys.* **2006**, *125,* 1941011-19410118.
[31] Zhao, Y.; Truhlar, D. G. *Theor. Chem. Acc.***2008**, *120*, 215-241.
[32] Zhao, Y.; Truhlar, D. G. *Acc. Chem. Res.* **2008**, *41*, 157-167.
[33] Domingos, S. R.; Luyten, H.; Anrooij, F. v.; Sanders, H. J.; Bakker, B. H.; Buma, W. J.; Hartl, F.; Woutersen, S. *Rev. Sci. Instrum.* **2013**, *84*, 0331031-0331034.
[34] Matheu, R.; Neudeck, S.; Meyer, F.; Sala, X.; Llobet, A. *ChemSusChem*, **2016**, *9*, 3361-3369.
[35] Dismukes, G. C.; Brimblecombe, R.; Felton, G. A. N.; Pryadun, R. S.; Sheats, J. E.; Spiccia, L.; Swiegers, G. F. *Acc. Chem. Res.* **2009**, *42*, 1935-1943.
[36] Nocera, D. G. *Acc. Chem. Res.* **2012**, *45*, 767–776.
[37] Mognon, L.; Benet-Buchholz, J.; Llobet, A. *Inorg. Chem.* **2015**, *54*, 11948-11957.
[38] Li, F.; Li, L.; Tong L.; Daniel, Q.; Gothelid, M.; Sun, L. *Chem. Commun.* **2014**, *50*, 13948-13951.
[39] Vigara, L.; Ertem, M. Z.; Planas, N.; Bozoglian, F.; Leidel, N.; Dau, H.; Haumann, M.; Gagliardi, L.; Cramer, C. J.; Llobet, A. *Chem. Sci.* **2012**, *3*, 2576-2586.
[40] Hirahara, M.; Ertem, M. Z.; Komi, M.; Yamazaki, H.; Cramer, C. J.; Yagi, M. *Inorg. Chem.* **2013**, *52*, 6354-6364.

TOC